Received: 7 December 2023 | Revised: 14 January 2024 | Accepted: 25 January 2024

DOI: 10.1002/elt2.29

RESEARCH ARTICLE

WILEY

Crystallinity engineering of carbon nitride protective coating for ultra-stable Zn metal anodes

Chen Liu[1,2,3] | Yuxin Zhu[4] | Shuanlong Di[4] | Jiarui He[4] | Ping Niu[1,2] | Antonios Kelarakis[5] | Marta Krysmann[6] | Shulan Wang[4] | Li Li[1,2,3]

[1]School of Metallurgy, Northeastern University, Shenyang, China

[2]State Key Laboratory of Rolling and Automation, Northeastern University, Shenyang, China

[3]Foshan Graduate School of Innovation, Northeastern University, Foshan, China

[4]Department of Chemistry, College of Science, Northeastern University, Shenyang, China

[5]UCLan Research Centre for Smart Materials, School of Natural Sciences, University of Central Lancashire, Preston, UK

[6]School of Dentistry, University of Central Lancashire, Preston, UK

Correspondence

Li Li and Antonios Kelarakis.
Email: lilicmu@alumni.cmu.edu and AKelarakis@uclan.ac.uk

Funding information

National Natural Science Foundation of China, Grant/Award Number: 22378055; Applied Basic Research Program of Liaoning, Grant/Award Number: 2022JH2/101300200; Guangdong Basic and Applied Basic Research Foundation, Grant/Award Number: 2022A1515140188; Fundamental Research Funds for the Central Universities, Grant/Award Numbers: N2002005, N2125004, N2225044, N232410019

Abstract

Ineffective control of dendrite growth and side reactions on Zn anodes significantly retards commercialization of aqueous Zn-ion batteries. Unlike conventional interfacial modification strategies that are primarily focused on component optimization or microstructural tuning, herein, we propose a crystallinity engineering strategy by developing highly crystalline carbon nitride protective layers for Zn anodes through molten salt treatment. Interestingly, the highly ordered structure along with sufficient functional polar groups and pre-intercalated K^+ endows the coating with high ionic conductivity, strong hydrophilicity, and accelerated ion diffusion kinetics. Theoretical calculations also confirm its enhanced Zn adsorption capability compared to commonly reported carbon nitride with amorphous or semi-crystalline structure and bare Zn. Benefiting from the aforementioned features, the as-synthesized protective layer enables a calendar lifespan of symmetric cells for 1100 h and outstanding stability of full cells with capacity retention of 91.5% after 1500 cycles. This work proposes a new conceptual strategy for Zn anode protection.

KEYWORDS

crystalline carbon nitride, crystallinity engineering, long cycling life, uniform Zn deposition, Zn metal anode

1 | INTRODUCTION

Aqueous Zn-ion batteries (ZIBs) hold great promise for large-scale sustainable energy storage owing to their low cost, environmental benign and high safety characteristics.[1,2] The Zn metal anode is considered as one of the most attractive anodes for ZIBs because of the high theoretical capacity (820 mAh g^{-1}), low redox potential (−0.76 V vs. standard hydrogen electrode), and simple scalable configurations.[3,4]

However, it strongly suffers from poor cycling stability during plating/stripping process and unavoidable surface corrosion in acidic electrolytes.[5,6] Especially, the notorious dendrite growth can puncture the separator and thus cause short-circuit failure and severe safety issues. How to achieve the effective Zn anode protection with rational design is currently the bottleneck issue for the development of high performance ZIBs.

Modification of the electrolyte/anode interface is viewed as the key avenue for achieving the effective protection of Zn metal anode while several corresponding strategies, including electrolyte engineering,[7] separator modification,[8] electrode texture regulation,[9] etc., have been developed. Among them, introducing the artificial interface layer on the surface of Zn metal anode for preventing its direct contact with an electrolyte and limiting dendrite growth is straightforward with potential high scalability.[10] Different coating materials have been attempted for serving as the interface layer but the performances of batteries still have a large space for improvement. For example, inorganic coatings with intrinsic fragile nature and weak bonding with Zn anode cannot maintain the mechanical stability during the repeated plating/stripping and have the peel-off risk,[11] while organic materials always suffer from low ionic conductivity which sets the significant barriers for rapid and uniform Zn^{2+} deposition.[12–14] As the emerging artificial-polymeric 2D material, graphitic carbon nitride with intrinsic triangular nanopores, and high content N sites for interacting with metal ions have attracted considerable interests in energy storage fields.[15] However, the most commonly reported C_3N_4 (CN) obtained from polymerization of N-rich precursors presents the melon structure composed of Zigzag chains, which is considered as the amorphous or semi-crystalline material.[16,17] More importantly, its low crystallinity with disordered structure hinders the transfer of metal ions with sluggish kinetics and causes high polarization with large interface resistance, which will dramatically deteriorate the performances of batteries.[18,19] Despite the encouraging progress for the design of protective layers, there is still a serious lack of fundamental understandings on the influence of inherent properties of coating materials on the microstructural and electrochemical performances of zinc anodes, which strongly retard the development of high-performance ZIBs.

Herein, we develop a crystallinity engineering strategy of Zn anode protection for the first time with synthesizing the highly crystalline carbon nitride (CCN) through the molten salt protocol. CCN was used as the interfacial layer to regulate the electrode/electrolyte interface for tuning the zinc deposition. Different from reported peer materials along with typical C_3N_4, the as-synthesized CCN with the featured structure of poly (heptazine imide) (PHI), the highly crystalline phase of g-C_3N_4,[16,20] combines the advantages of both inorganic materials for high ionic/electrical conductivity as the carbonaceous derivative and organic materials with high flexibility and mechanical strength as the artificial polymer. The detailed features of this strategy and our design principle are presented in Figure 1: (1) owing to its highly ordered structure and improved conductivity, the use of CCN is beneficial for homogenizing electrical field distribution and elevating ion diffusion kinetics with reduced interfacial resistance, which is crucial for achieving the uniform Zn deposition; (2) the abundant surface functional polarization groups can enhance the hydrophilicity with decreased desolvation barrier and suppressed side reactions for the formation of even zinc nucleation; and (3) the

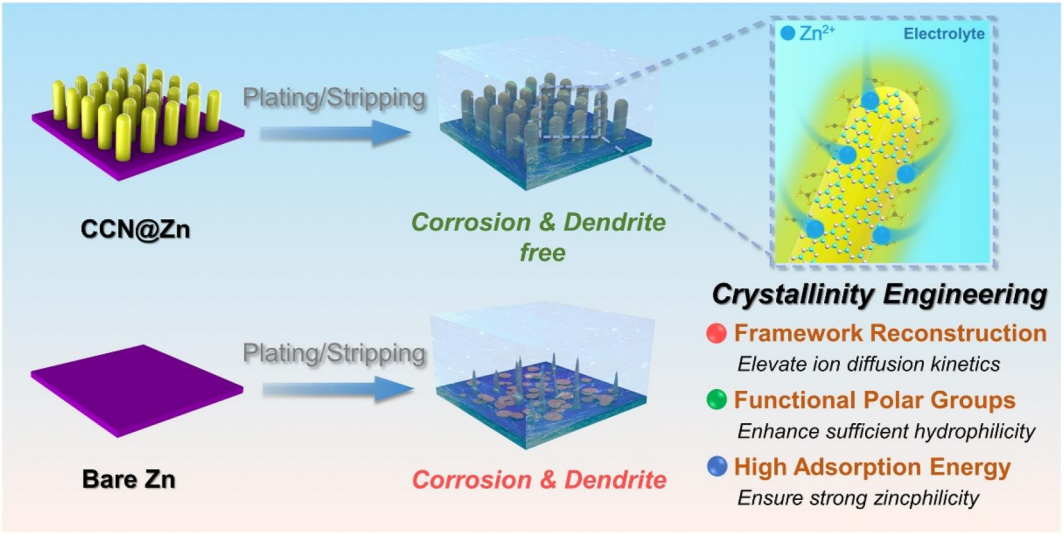

FIGURE 1 The design principle for protecting the Zn anode based on the crystallinity engineering strategy.

high Zn adsorption capability from its highly crystalline structure ensures strong zincphilicity and high-strength interactions with Zn^{2+} for effectively regulating the ion flux and enhancing the transfer rate. Profiting from these advantageous features, the assembled cell delivered an outstanding prolonged lifespan and excellent Zn plating/stripping reversibility for 1100 h as well as the outstanding full-cell capacity retention of 91.5% after 1500 cycles.

2 | RESULTS AND DISCUSSION

2.1 | Prediction of Zn adsorption capability and microstructural characterizations

Density functional theory (DFT) calculations were first conducted to evaluate the adsorption energies of CN and CCN during Zn deposition process (Figure 2A). It can be clearly observed that the calculated adsorption energy of Zn atom adsorbed on CCN (−1.8 eV) is significantly higher than that of CN (−0.85 eV) and bare Zn (001) (−0.25 eV), demonstrating that the CCN presents enhanced adsorption ability for capturing the Zn atom and thus elevated zincophilicity for achieving uniform Zn deposition.[21] Inspired by this result, we believe CCN designed from crystallinity engineering may achieve the effective protection of Zn anode and thus the corresponding preparation was conducted subsequently with the detailed morphological and structural analysis performed. Due to the stable physicochemical properties, a mixture of LiCl, KCl, and NaCl was selected as the processing media.[22,23] CCN was prepared through molten salt processing of pristine CN, which creates a liquid environment to induce the structural ordering of CN intermediates and increases crystallinity.[16,24] The crystallinity enhancement of CCN can be clearly confirmed by the presence of a peak at 8.1° in the X-ray diffraction pattern (Figure 2B), which is the characteristic peak of PHI, the highly crystalline phase of carbon nitride, with enlarged in-plane periodicity.[25] Meanwhile, its strongest peak at 28.2° that represents layered stacking of C_3N_4 shows a right-shift trend compared with that in CN, which indicates its contracted interlayer distance and stronger interlayer interaction.[26] The full width at half maximum analysis also reveals that CCN shows the smaller value, further demonstrating the crystallinity enhancement of CCN (Table S1). The extended condensed structure with narrowed layer spacing arising from crystallinity engineering is beneficial for reducing the interlayer barrier of protective coating and accelerating its ions diffusion kinetics. Fourier-transform infrared spectroscopy (FT-IR) was then conducted to investigate the structural changes and chemical compositions of CN and CCN (Figure 2C). The peak of uncondensed terminal amino group ranging from 3500 to 2900 cm^{-1} is significantly weakened in the spectrum of CCN, demonstrating its highly crystalline structure with complete condensation of adjacent heptazine units.[27] Meanwhile, a new peak at 2170 cm^{-1} due to the introduction of polar cyano groups along with the signal of K^+ from molten salt at 1000 cm^{-1} can also be found for CCN, which are viewed as featured peaks of PHI.[28] The presence of polar cyano groups is beneficial for decreasing the desolvation energy barrier of Zn^{2+} deposition and facilitating Zn^{2+} diffusion kinetics.[29] The crystallinity of CN was increased by high-temperature molten salt treatment, which induces structure reconstruction and promotes crystallization kinetics by facilitating hydrogen bond breaking and deamination to transform CN with the melon structure composed of Zigzag chains into CCN with highly ordered structure. Impressively, the contact angle measurement is different from the CN layer which increased the values from 98.2° (bare Zn) to 142.8° (CN@Zn); CCN@Zn electrode presented a smaller contact angle (74.3°) with enhanced hydrophilicity, which is favorable for promoting ion transport through the protective layer (Figure 2D).[30]

The scanning electron microscope (SEM) images show the presence of apparent scratches and protrusions on the surface of bare Zn foil (Figure 2E), which is prone to cause the uneven distribution of Zn^{2+} concentration and accelerate the growth of dendrites. The coating of CN with large bulk (Figure S1) is uneven and loose (Figure 2F), which may cause the "tip effect" for dendrite formation and the occurrence of side reactions.[31] In contrast, the CCN dense layer composed of continuous nanorods in the diameter of 60 nm (Figure S2) was coated uniformly on the Zn foil with great integrity (Figure 2G), which can offer abundant active sites with large contact area to electrolytes and is favorable for achieving even Zn deposition. After molten salt treatment, the specific surface area of CCN can be significantly increased due to the microstructure evolution from CN with sheet/bulk morphology to CCN with rod-like morphology.[32] The coating thickness of CCN layer is approximately 16.7 μm with the homogeneous distribution of elements (Figure 2H). Additionally, no stripping or cracks were observed on the CCN layer after the repeated bending test, proving its stable mechanical properties and intimate contact with the Zn foil (Figure S3).

2.2 | Electrochemical performances of symmetric and asymmetrical cells

The stability and reversibility of zinc electrodes were evaluated by assembling Zn||Zn symmetric cells. For

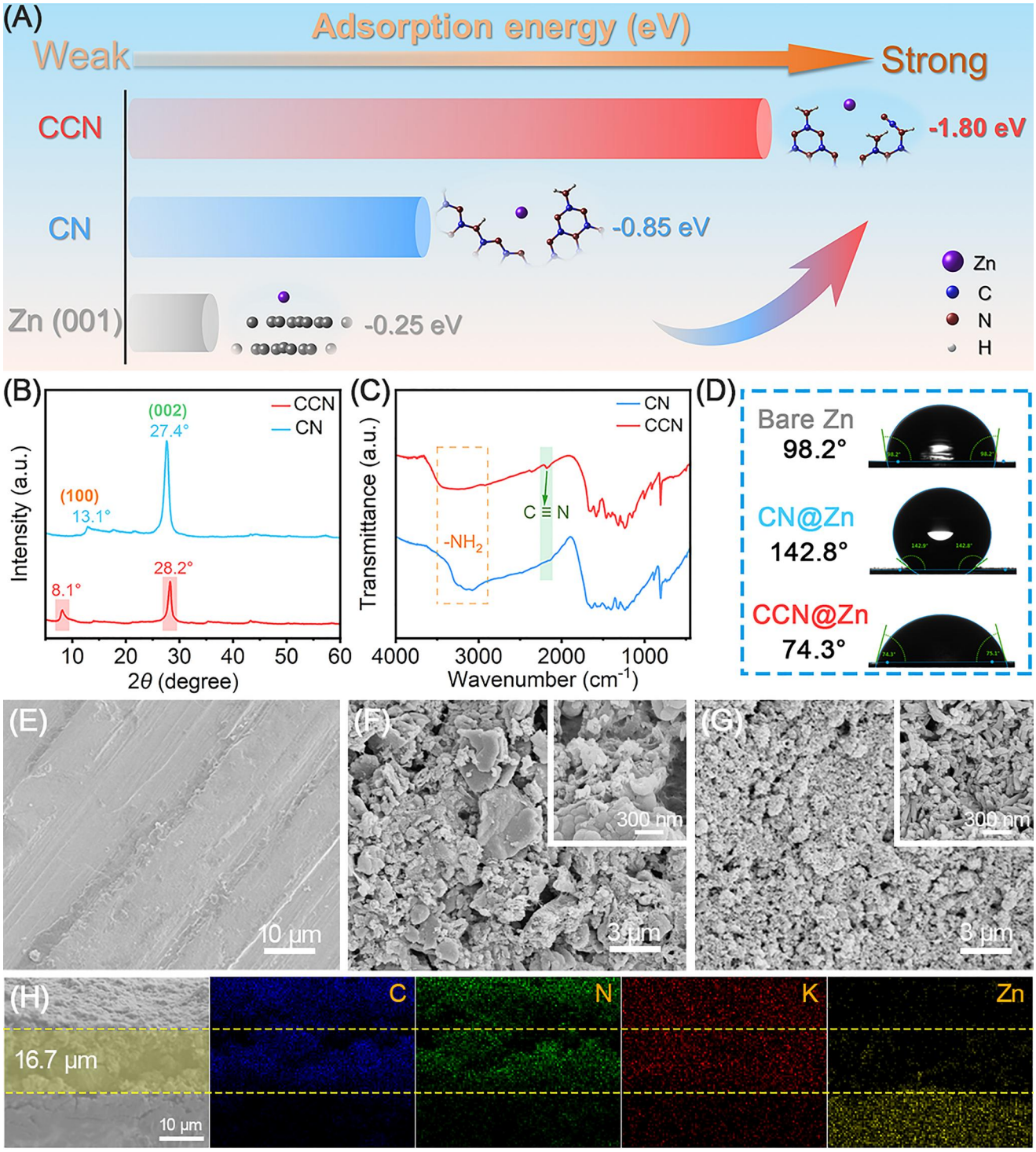

FIGURE 2 (A) Adsorption energies of the Zn atom on Zn (001), CN and CCN calculated through density functional theory, respectively. (B) X-ray diffraction patterns and (C) Fourier-transform infrared spectroscopy spectra of CN and CCN. (D) Contact angle measurements of an electrolyte on bare Zn, CN@Zn and CCN@Zn electrodes. SEM images of (E) bare Zn, (F) CN@Zn and (G) CCN@Zn electrodes. (H) Cross-sectional SEM image and the corresponding elemental mappings of the CCN@Zn electrode. CCN, crystalline carbon nitride; CN, carbon nitride; SEM, scanning electron microscope.

symmetric cells of bare Zn, a sudden rise in polarization voltage was observed after cycling for 230 h due to the serious side reactions and dendrite growth (Figure 3A). Correspondingly, the CN@Zn symmetric cell can run for 800 h with limited protection at the moderate current and deposition density of 1 mA cm^{-2} and 1 mAh cm^{-2}. In contrast, the symmetric cell with CCN layer exhibited ultralong

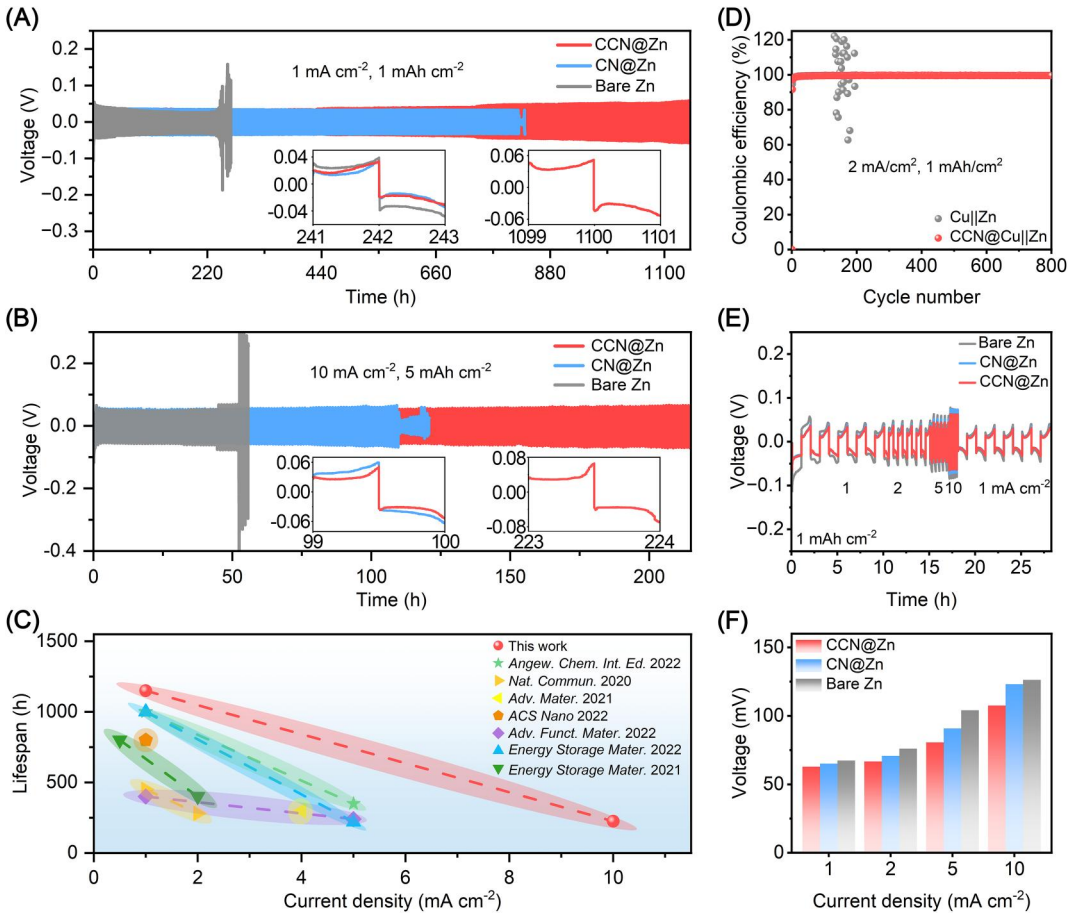

FIGURE 3 Cycling performance of symmetrical cells with bare Zn, CN@Zn and CCN@Zn electrodes at (A) 1 mA cm^{-2} and 1 mAh cm^{-2}; and (B) 10 mA cm^{-2} and 5 mAh cm^{-2}. (C) Comparison of lifespan of the CCN@Zn electrode with recently reported peer samples at different current densities. (D) Coulombic efficiencies of Zn plating/stripping on bare Zn and CCN@Zn electrodes at 2 mA cm^{-2} and 1 mAh cm^{-2}. (E) Rate performance of symmetric cells at different current densities from 1 to 10 mA cm^{-2}, and (F) the corresponding voltage hysteresis.

stability even over 1100 h without apparent decay, unfolding its excellent Zn plating/stripping reversibility. Similarly, when the current densities were increased to 2 and 5 mA cm^{-2}, CCN@Zn still presented outstanding cycling stability over 900 h (Figures S4 and S5). Furthermore, even at the high current density of 10 mA cm^{-2} with a deposition capacity of 5 mAh cm^{-2}, the CCN@Zn symmetric cell still showed high reversibility and prolonged lifespan of repeated plating/stripping process over 220 h, which is much better than its counterparts of CN@Zn and bare Zn, further highlighting its outstanding inhibition capability on the parasitic reactions and dendrite growth (Figure 3B). To the best of our knowledge, the performances of CCN surpasses those of many previously reported peer samples and are among the highest values in all reported ZIB anode protection layers (Figure 3C, Table S2).[33–39]

The role of CCN layer is further analyzed by evaluating the assembled Cu||Zn asymmetrical cells. As shown in Figure 3D, long cycling life (800 cycles) with high average Coulombic efficiency (CE) of 99.5% was delivered for CCN@Cu||Zn at 2 mA cm^{-2}, which demonstrates the excellent ability of CCN layer for Zn flux regulation compared with its reported counterparts (Table S3). The diffusion kinetics of Zn^{2+} is also significantly improved with a stable voltage fluctuation and low gap achieved (Figures S6 and S7).[29] As the comparison, the bare Cu||Zn cell displayed the fluctuated CE and then failed due to the internal short-circuit even within only 130 cycles. The rate performance evaluation of symmetric cells at different current densities was carried out with a fixed capacity of 1 mAh cm^{-2} (Figure 3E). It can be observed the CCN@Zn based cell showed superior rate performance with lower voltage hysteresis to the other controls. Even at the high current density of 10 mA cm^{-2}, it displayed the lowest voltage hysteresis of 107.5 mV, outperforming the samples with CN@Zn (123.1 mV) and bare Zn (126.2 mV) electrodes (Figure 3F). The aforementioned results of electrochemical performances confirm the crucial role of

CCN layer for ensuring superior rate capability and excellent cycling stability during the repeated Zn plating/stripping process. Electrochemical impedance spectroscopy was performed to further investigate the ionic conductivity of CCN, while a lower charge-transfer resistance (R_{ct}) demonstrates more rapid Zn^{2+} diffusion kinetics and superior ionic conductivity.[10] As shown in Figure S8, the CCN@Zn symmetric cell delivered a lower R_{ct} value of 534.4 Ω than that of CN (749.1 Ω) and bare Zn (1061.1 Ω) counterparts, indicating the enhanced ion diffusion kinetics and robust ionic conductivity of the CCN layer.

2.3 | Investigation of electrochemical stripping/plating behaviors

To visually evaluate the dendrite inhibition ability endowed by CCN layer, in situ optical microscope was conducted to monitor the behaviors of Zn deposition at 10 mA cm^{-2} (Figure 4A). It can be clearly observed that the heterogeneous protrusions gradually appeared on the surface of bare Zn electrode through test duration with the formation of uneven deposits and then the dendrites. As a comparison, a uniform and smooth Zn deposition without dendrite growth was found for CCN@Zn electrode throughout the whole 60-min plating process, demonstrating the excellent Zn^{2+} flux regulation capability of CCN layer. Meanwhile, CCN layer is firmly bonded with Zn foil without coating loss or stripping observed, which also confirms its high chemical stability and outstanding resistance to the volume expansion during the repeated plating/stripping. The 3D laser confocal scanning microscope further intuitively compared the different surface situations between bare Zn and CCN@Zn electrodes. The apparent protrusions with uneven Zn deposition (Figure 4B) were observed on bare Zn while smooth surface with effectively suppressed Zn dendrites were presented for its CCN@Zn counterpart (Figure 4C). The subsequent SEM investigation for the cycled electrodes reveal that a mass of flaky by-products with uncontrolled dendrites in different dimensions were generated on the surface of bare Zn electrode, which tends to cause short-circuit of ZIBs (Figure 4D, F). In sharp contrast, the surface of CCN@Zn electrode after cycling is dense and flat without any dendrite and rupture, confirming the strong regulation capability of CCN layers for plating/stripping behaviors and their excellent mechanical stability during the long-term cycles (Figure 4E,G). Moreover, as shown in Figure 4E, no Zn deposits can be observed on the surface of the CCN layer after cycling, indicating that Zn deposition occurs below the layer due to its high ionic conductivity, which can effectively prevent Zn dendrite growth and mitigate the corrosions (Figure 4E). Chronoamperometry with an applied overpotential of −150 mV was employed to explore the nucleation behavior and deposition mode of electrodes (Figure S9). Bare Zn anode showed disordered 2D planar diffusion mode with the current increasing directly during the testing, which indicates that Zn^{2+} tends to diffuse laterally along the electrode surface to a specific location with low nucleation barrier and thus preferably form the dendrites.[40] Alternatively, Zn^{2+} presented a transitory 2D diffusion on the surface of CCN@Zn electrode within the initial 40 s, following with a new 3D diffusion process at the later time that indicates the in situ deposition of diffused Zn^{2+}. This result is consistent with the aforementioned microscopic observations and also demonstrates the diffusion kinetics changes with the presence of CCN layers for controlling the even distribution of Zn^{2+}.

2.4 | Discoloration phenomenon investigation and theoretical analysis

Homogenized Zn^{2+} flux with high transference across the protective layer is essential for achieving the uniform deposition of zinc ions. As the organic polymeric semiconductor, CCN with sufficient polar surface cyano (—C≡N) groups, as confirmed by the FT-IR results shown in Figure 2C, can lower the desolvation energy of Zn^{2+} for reducing its combination with H_2O and homogenize Zn^{2+} flux.[41] More interestingly, the presence of intercalated K^+ derived from molten salt in CCN can exchange with the desolvated Zn^{2+} to reduce the direct access of H_2O to zinc anode surface, thus effectively decreasing its side reactions while maintaining high Zn^{2+} transference. To confirm this, a typical discoloration experiment with CCN@Zn electrode immersed in different electrolytes was designed. The color of electrodes changed from yellow to blue (Figure 5A) in the 2 M $ZnSO_4$ electrolyte while no color change of electrodes was observed in water (Figure S10), demonstrating the occurrence of ion-exchange between K^+ and Zn^{2+}. Furthermore, the inductively coupled plasma optical emission spectroscopy was conducted to detect changes in content of K element before and after soaking the CCN@Zn electrode in the 2 M $ZnSO_4$ electrolyte, where the result shows that the content of K element increases, validating aforementioned hypothesis of ion-exchange (Table S4). Correspondingly, no color change was observed for CN@Zn or bare Zn electrode when it was immersed in the $ZnSO_4$ electrolyte (Figure S10). The discoloration phenomenon of the CCN@Zn electrode can even be observed through the separator when assembling the coin cells (Figure S11).

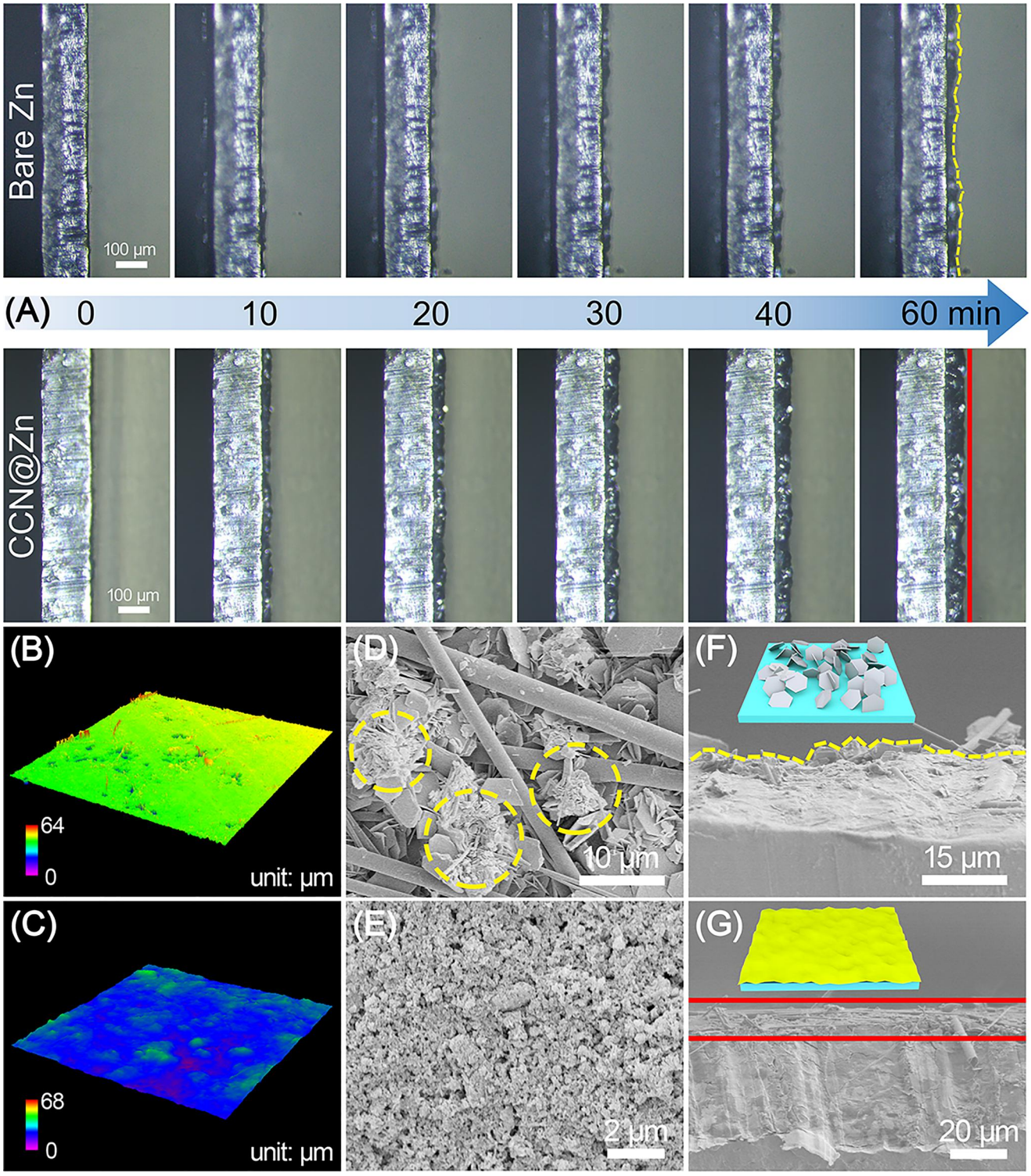

FIGURE 4 (A) In situ optical microscopy observation of Zn plating on bare Zn and CCN@Zn electrodes at 10 mA cm^{-2}. (B, C) Laser confocal microscope images, (D, E) top-view SEM images, and (F, G) cross-sectional SEM images of bare Zn and CCN@Zn electrodes after 50 cycles at 1 mA cm^{-2} and 1 mAh cm^{-2}. SEM, scanning electron microscope.

The cross-sectional SEM analysis along with EDS mappings for the soaked CCN@Zn electrode shows that Zn element is uniformly distributed through the CCN layer (Figure 5B), confirming the critical role of CCN as ion-distributor for homogenizing Zn ion flux and regulating its deposition kinetics. The theoretical analysis based on DFT calculations reveals that CCN presents the strongest adsorption capacity for Zn^{2+}

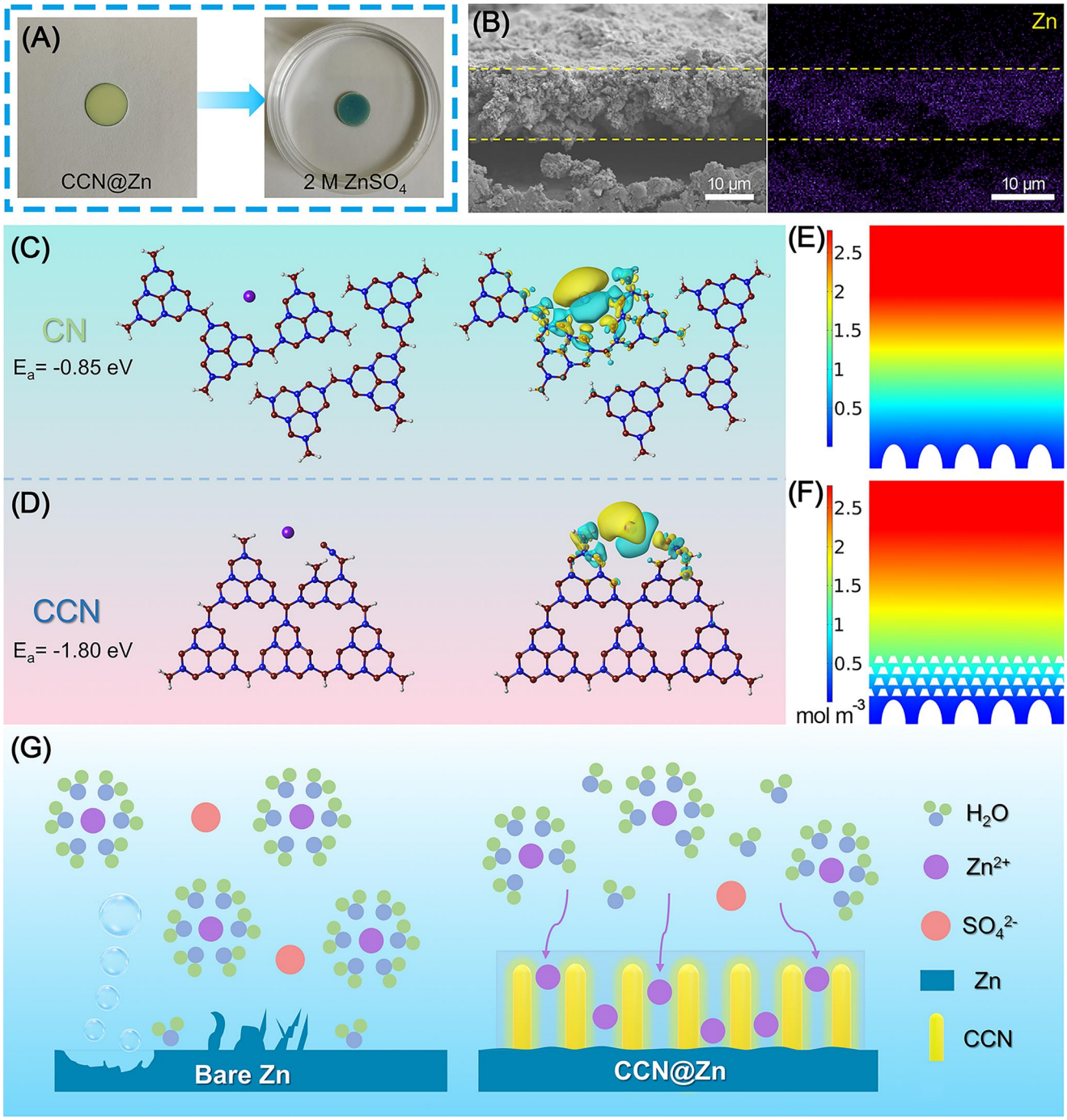

FIGURE 5 (A) Digital images of CCN@Zn electrodes for immersion into the 2 M $ZnSO_4$ electrolyte to check the color change. (B) Cross-sectional scanning electron microscope image and the corresponding elemental mapping of immersed the CCN@Zn electrode. (C, D) Optimized density functional theory calculation models with the adsorption energy of Zn atom adsorbed on CN and CCN marked as well as the corresponding differential charge density distribution. Zn^{2+} ion field simulation for (E) bare Zn and (F) CCN@Zn electrodes. (G) Schematic illustration of the Zn^{2+} deposition process on bare Zn and CCN@Zn electrodes. CCN, crystalline carbon nitride; CN, carbon nitride.

(−1.80 eV) compared with CN (−0.85 eV) (Figure 5C, D) and bare Zn (Figure S12), which can effectively prevent the transfer of deposited Zn^{2+} to the favorable nucleation sites for the formation of dendrites. This result is consistent with the experimental phenomenon that the CCN-based electrode shows the highest zincophilicity. COMSOL Multiphysics software was used to simulate the effect of the protective layer on controlling the distribution of Zn ions. It can be clearly observed that a gradient ion distribution was formed for bare Zn (Figure 5E), which promotes ion aggregation and is liable to form the dendrites. In

contrast, the CCN@Zn electrode shows the even distribution of zinc ions without apparent gradient patterns (Figure 5F), which is consistent with the uniform deposition of Zn^{2+} as obtained through the experimental evidences. A schematic of Zn deposition on the surface of the CCN@Zn electrode was illustrated in Figure 5G. The protective layer with high chemical stability prevents direct contact between water and the electrode, which inhibits the water-induced side reactions and corrosion. Meanwhile, the effective ion-exchange between K^+ and Zn^{2+} along with the abundant surface polar group allows CCN as the ion-distributor to regulate the diffusion of zinc ions with accelerated desolvation process while maintaining the high flux for uniform deposition. High crystallinity with high ionic conductivity can also facilitate the deposition kinetics. The aforementioned characteristics explain the excellent protection of Zn metal anodes based on CCN, which may lead to the performance elevation of full-cell performances.

2.5 | Full-cell performances

The full-cell was then assembled with the as-prepared CCN@Zn as the anode and typical MnO_2 (Figures S13 and S14) as the cathode. Based on the cyclic voltammetry (CV) curves at a scan rate of 0.1 mV s^{-1} (Figure 6A), two pairs of redox peaks corresponding to the two-step reverse oxidation/reduction between MnO_2 and MnOOH can be observed.[41] The shape similarity of these two peaks demonstrates that CCN only serves as the functional protective layer but does not get involved into the electrochemical reactions, which is highly preferred for surface modification related strategies.[42] Meanwhile, compared with the bare Zn-related full cell counterpart, the CCN@Zn||MnO_2 presented a smaller voltage polarization for oxidation/reduction peaks, confirming its expedited ion diffusion kinetics which was also confirmed in the half-cell configuration.[43] The corresponding discharge–charge profiles showed the platforms at 1.57, 1.39, and 1.25 V,

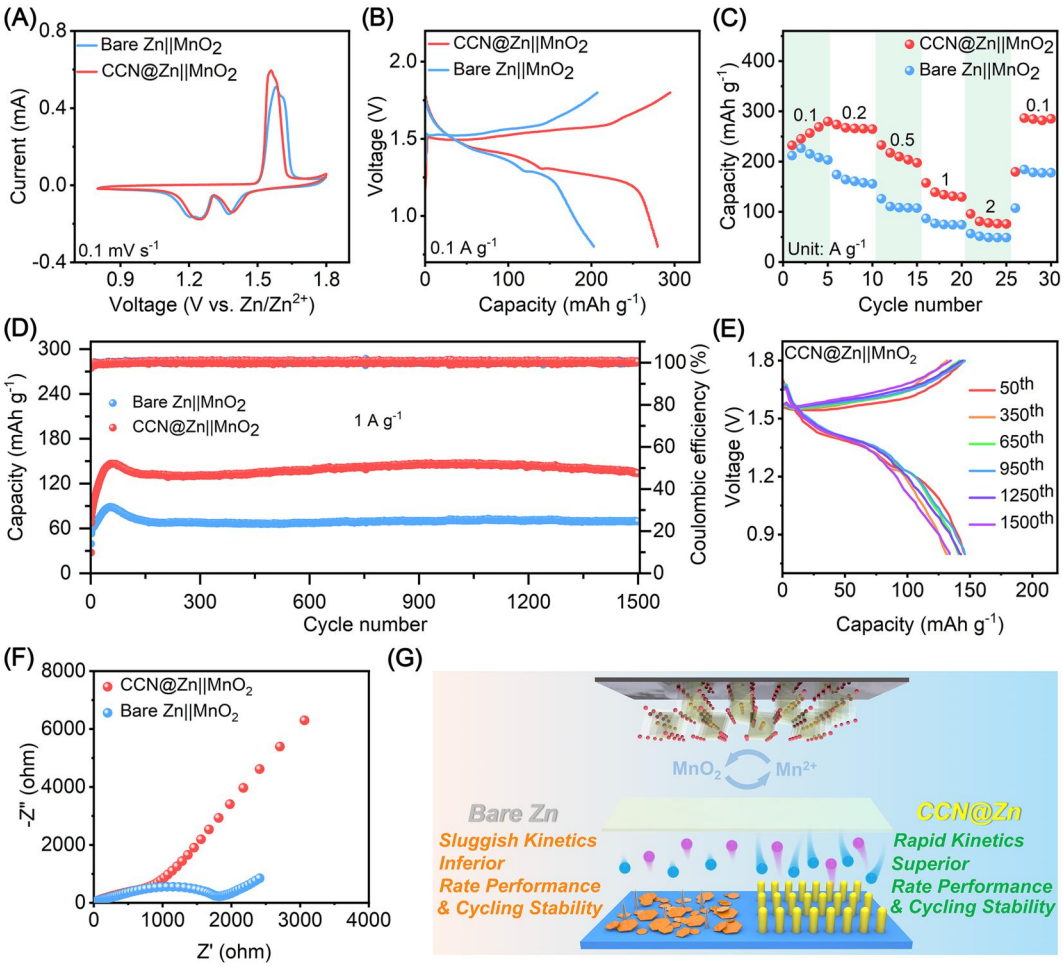

FIGURE 6 Electrochemical performance comparison of Zn||MnO_2 full cells with bare Zn and CCN@Zn anodes: (A) CV curves at 0.1 mV s^{-1}, (B) charge/discharge curves at 0.1 A g^{-1}, (C) rate performances, and (D) cycling stability at 1 A g^{-1}. (E) Charge/discharge curves of CCN@Zn||MnO_2 full cells with different cycles at 1 A g^{-1}. (F) Electrochemical impedance spectroscopy spectra of full cells with bare Zn and CCN@Zn anodes. (G) Illustration of the bare Zn and CCN@Zn related full cells during long-term plating/stripping. CV, cyclic voltammetry.

which is consistent with the CV curve (Figure 6B). It also delivered a full-line lifted rate capacities ranging from 0.1 to 2 A g^{-1} compared with bare Zn (Figure 6C) and CN related full cell (Figure S15). CCN@Zn||MnO_2 can also maintain a high capacity retention of 133.8 mAh g^{-1} (91.5%) after 1500 cycles, which is superior to the control bare Zn||MnO_2 that only delivered 69.5 mAh g^{-1} with a capacitance retention of 78.7% (Figure 6D). Its lower voltage polarization (Figure 6E) than the bare Zn||MnO_2 counterpart (Figure S16) within 1500 cycles along with the smaller charge transfer resistance (R_{ct}: 311.3 Ω (CCN@Zn) versus 1972.2 Ω (bare Zn)) (Figure 6F, Figure S17, Table S5) further reveals the stabilized electrochemical performances with fast Zn^{2+} diffusion kinetics of CCN related batteries.[44] A schematic diagram of bare Zn and CCN@Zn related full cells during long cycling process to highlight the critical role of CCN for electrode protection and performance enhancement was presented in Figure 6G.

3 | CONCLUSION

In summary, we developed a crystallinity engineering-related strategy for Zn anode protection. Highly crystalline C_3N_4 with the structure of PHI and strong Zn^{2+} adsorption capacity was used as the interfacial layer. Compared with the bare Zn and commonly reported polymeric C_3N_4, its highly ordered structure with fully condensed network and reduced layer spacing ensures rapid Zn^{2+} diffusion kinetics and high ionic conductivity while the abundant polar surface cyano groups and pre-intercalated K^+ also endow CCN with the ion-distribution capability for dendrites regulation and side reaction inhibition. The CCN@Zn symmetric cell therefore achieved the ultralong stability for 1100 h at 1 mA cm^{-2}, 1 mAh cm^{-2}, and 220 h even at 10 mA cm^{-2} and 5 mAh cm^{-2} with the average CE of 99.5% after 800 cycles, which are among the highest values for reported Zn protection layers. When assembling as the full cell of CCN@Zn||MnO_2, it can deliver outstanding rate capability and superior cycling stability with capacity retention of 91.5% after 1500 cycles. This work provides a new strategy by designing an advanced dendrite-free interface layer for the ultra-stable Zn metal anode based on crystallinity engineering and extends the use of C_3N_4 related materials for high-performance batteries.

ACKNOWLEDGMENTS

This work was supported by the National Natural Science Foundation of China (22378055), the Applied Basic Research Program of Liaoning (2022JH2/101300200), the Guangdong Basic and Applied Basic Research Foundation (2022A1515140188), Fundamental Research Funds for the Central Universities (N2002005, N2125004, N2225044, and N232410019). We also appreciate the instrumental analysis from Analytical and Testing Center, Northeastern University.

CONFLICT OF INTEREST STATEMENT

The authors declare no competing interests.

ORCID

Li Li https://orcid.org/0000-0003-2308-916X

REFERENCES

1. Zhang N, Wang J-C, Guo Y-F, Wang P-F, Zhu Y-R, Yi T-F. Insights on rational design and energy storage mechanism of Mn-based cathode materials towards high performance aqueous zinc-ion batteries. *Coord Chem Rev*. 2023;479:215009. https://doi.org/10.1016/j.ccr.2022.215009
2. Liu H, Cai X, Zhi X, et al. An amorphous anode for proton battery. *Nano-Micro Lett*. 2022;15(1):24. https://doi.org/10.1007/s40820-022-00987-2
3. Zhang N, Chen X, Yu M, Niu Z, Cheng F, Chen J. Materials chemistry for rechargeable zinc-ion batteries. *Chem Soc Rev*. 2020;49(13):4203-4219. https://doi.org/10.1039/c9cs00349e
4. Verma V, Chan RM, Yang LJ, et al. Chelating ligands as electrolyte solvent for rechargeable zinc-ion batteries. *Chem Mater*. 2021;33(4):1330-1340. https://doi.org/10.1021/acs.chemmater.0c04358
5. Hao J, Yuan L, Ye C, et al. Boosting zinc electrode reversibility in aqueous electrolytes by using low-cost antisolvents. *Angew Chem Int Ed*. 2021;60(13):7366-7375. https://doi.org/10.1002/anie.202016531
6. Ma L, Li Q, Ying Y, et al. Toward practical high-areal-capacity aqueous zinc-metal batteries: quantifying hydrogen evolution and a solid-ion conductor for stable zinc anodes. *Adv Mater*. 2021;33(12):2007406. https://doi.org/10.1002/adma.202007406
7. Shi X, Wang J, Yang F, Liu X, Yu Y, Lu X. Metallic zinc anode working at 50 and 50 mAh cm^{-2} with high depth of discharge via electrical double layer reconstruction. *Adv Funct Mater*. 2023;33(7):2211917. https://doi.org/10.1002/adfm.202211917
8. Fang Y, Xie X, Zhang B, et al. Regulating zinc deposition behaviors by the conditioner of PAN separator for zinc-ion batteries. *Adv Funct Mater*. 2022;32(14):2109671. https://doi.org/10.1002/adfm.202109671
9. Yi Z, Liu J, Tan S, et al. An ultrahigh rate and stable zinc anode by facet-matching-induced dendrite regulation. *Adv Mater*. 2022;34(37):2203835. https://doi.org/10.1002/adma.202203835
10. Huo X, Xu L, Xie K, et al. Cation-selective interface for kinetically enhanced dendrite-free Zn anodes. *Adv Energy Mater*. 2023;13(20):2203066. https://doi.org/10.1002/aenm.202203066
11. Liu H, Ye Q, Lei D, et al. Molecular brush: an ion-redistributor to homogenize fast Zn^{2+} flux and deposition for calendar-life Zn batteries. *Energy Environ Sci*. 2023;16(4):1610-1619. https://doi.org/10.1039/d2ee03952d
12. Di S, Nie X, Ma G, et al. Zinc anode stabilized by an organic-inorganic hybrid solid electrolyte interphase. *Energy Storage Mater*. 2021;43:375-382. https://doi.org/10.1016/j.ensm.2021.09.021
13. Wang Y, Li H, Chen S, et al. An ultralong-life SnS-based anode through phosphate-induced structural regulation for high-performance sodium ion batteries. *Sci Bull*. 2022;67(20):2085-2095. https://doi.org/10.1016/j.scib.2022.09.021
14. Wang Y, Niu P, Li J, Wang S, Li L. Recent progress of phosphorus composite anodes for sodium/potassium ion

batteries. *Energy Storage Mater*. 2021;34:436-460. https://doi.org/10.1016/j.ensm.2020.10.003
15. Wang J, Liu Z, Qu B, et al. g-C_3N_4 in situ derived ionic-electronic dual-conducting interlayer with N-rich sites for long lifespan sodium metal anodes. *Energy Storage Mater*. 2023;59:102793. https://doi.org/10.1016/j.ensm.2023.102793
16. Zhai B, Li H, Gao G, et al. A crystalline carbon nitride based near-infrared active photocatalyst. *Adv Funct Mater*. 2022;32(47):2207375. https://doi.org/10.1002/adfm.202207375
17. Di S, Li H, Zhai B, et al. A crystalline carbon nitride-based separator for high-performance lithium metal batteries. *Proc Natl Acad Sci USA*. 2023;120(33):e2302375120. https://doi.org/10.1073/pnas.2302375120
18. Wang Y, Lin X, Wang L, Yang Y, Zhang Y, Pan A. Tailoring the crystal-chemical states of water molecules in sepiolite for superior coating layers of Zn metal anodes. *Adv Funct Mater*. 2023;33(13):2211088. https://doi.org/10.1002/adfm.202211088
19. Li H, Di S, Niu P, Wang S, Wang J, Li L. A durable half-metallic diatomic catalyst for efficient oxygen reduction. *Energy Environ Sci*. 2022;15(4):1601-1610. https://doi.org/10.1039/d1ee03194e
20. Lin L, Yu Z, Wang X. Crystalline carbon nitride semiconductors for photocatalytic water splitting. *Angew Chem Int Ed*. 2019;58(19):6164-6175. https://doi.org/10.1002/anie.201809897
21. Wang P, Liang S, Chen C, et al. Spontaneous construction of nucleophilic carbonyl-containing interphase toward ultra-stable zinc-metal anodes. *Adv Mater*. 2022;34(33):2202733. https://doi.org/10.1002/adma.202202733
22. Li H, Cheng B, Xu J, Yu J, Cao S. Crystalline carbon nitrides for photocatalysis. *EES Catal*. 2024. https://doi.org/10.1039/D3EY00302G
23. Mohan G, Venkataraman M, Gomez-Vidal J, Coventry J. Thermo-economic analysis of high-temperature sensible thermal storage with different ternary eutectic alkali and alkaline earth metal chlorides. *Sol Energy*. 2018;176:350-357. https://doi.org/10.1016/j.solener.2018.10.008
24. Sun K, Wang Y, Chang C, et al. Molten-salt synthesis of crystalline C_3N_4/C nanosheet with high sodium storage capability. *Chem Eng J*. 2021;425:131591. https://doi.org/10.1016/j.cej.2021.131591
25. Lin L, Ren W, Wang C, Asiri AM, Zhang J, Wang X. Crystalline carbon nitride semiconductors prepared at different temperatures for photocatalytic hydrogen production. *Appl Catal B Environ*. 2018;231:234-241. https://doi.org/10.1016/j.apcatb.2018.03.009
26. Wu S, Yu H, Chen S, Quan X. Enhanced photocatalytic H_2O_2 production over carbon nitride by doping and defect engineering. *ACS Catal*. 2020;10(24):14380-14389. https://doi.org/10.1021/acscatal.0c03359
27. Liang Y, Wu X, Liu X, Li C, Liu S. Recovering solar fuels from photocatalytic CO_2 reduction over W^{6+}-incorporated crystalline g-C_3N_4 nanorods by synergetic modulation of active centers. *Appl Catal B Environ*. 2022;304:120978. https://doi.org/10.1016/j.apcatb.2021.120978
28. Lin L, Ou H, Zhang Y, Wang X. Tri-*s*-triazine-based crystalline graphitic carbon nitrides for highly efficient hydrogen evolution photocatalysis. *ACS Catal*. 2016;6(6):3921-3931. https://doi.org/10.1021/acscatal.6b00922
29. Zhang H, Li S, Xu L, et al. High-yield carbon dots interlayer for ultra-stable zinc batteries. *Adv Energy Mater*. 2022;12(26):2200665. https://doi.org/10.1002/aenm.202200665
30. Ke J, Wen Z, Yang Y, et al. Tailoring anion association strength through polycation-anion coordination mechanism in imidazole polymeric ionic liquid-based artificial interphase toward durable Zn metal anodes. *Adv Funct Mater*. 2023;33(26):2301129. https://doi.org/10.1002/adfm.202301129
31. Wang S, Yuan C, Chang N, et al. Act in contravention: a non-planar coupled electrode design utilizing "tip effect" for ultra-high areal capacity, long cycle life zinc-based batteries. *Sci Bull*. 2021;66(9):889-896. https://doi.org/10.1016/j.scib.2020.12.029
32. Li Y, Wang B, Xiang Q-J, Zhang Q, Chen G. Alkali metal-modified crystalline carbon nitride for photocatalytic nitrogen fixation. *Dalton Trans*. 2022;51(43):16527-16535. https://doi.org/10.1039/d2dt02731c
33. Zhang Q, Luan J, Huang X, et al. Revealing the role of crystal orientation of protective layers for stable zinc anode. *Nat Commun*. 2020;11(1):3961. https://doi.org/10.1038/s41467-020-17752-x
34. Qiu M, Sun P, Wang Y, Ma L, Zhi C, Mai W. Anion-trap engineering toward remarkable crystallographic reorientation and efficient cation migration of Zn ion batteries. *Angew Chem Int Ed*. 2022;61(44):e202210979. https://doi.org/10.1002/anie.202210979
35. Zhu M, Hu J, Lu Q, et al. A patternable and in situ formed polymeric zinc blanket for a reversible zinc anode in a skin-mountable microbattery. *Adv Mater*. 2021;33(8):2007497. https://doi.org/10.1002/adma.202007497
36. Hong L, Wu X, Wang L-Y, et al. Highly reversible zinc anode enabled by a cation-exchange coating with Zn-ion selective channels. *ACS Nano*. 2022;16(4):6906-6915. https://doi.org/10.1021/acsnano.2c02370
37. Wang L, Huang W, Guo W, et al. Sn alloying to inhibit hydrogen evolution of Zn metal anode in rechargeable aqueous batteries. *Adv Funct Mater*. 2022;32(1):2108533. https://doi.org/10.1002/adfm.202108533
38. Cao Z, Zhu X, Xu D, et al. Eliminating Zn dendrites by commercial cyanoacrylate adhesive for zinc ion battery. *Energy Storage Mater*. 2021;36:132-138. https://doi.org/10.1016/j.ensm.2020.12.022
39. So S, Ahn YN, Ko J, Kim IT, Hur J. Uniform and oriented zinc deposition induced by artificial Nb_2O_5 Layer for highly reversible Zn anode in aqueous zinc ion batteries. *Energy Storage Mater*. 2022;52:40-51. https://doi.org/10.1016/j.ensm.2022.07.036
40. Hong L, Wang L-Y, Wang Y, et al. Toward hydrogen-free and dendrite-free aqueous zinc batteries: formation of zincophilic protective layer on Zn anodes. *Adv Sci*. 2022;9(6):2104866. https://doi.org/10.1002/advs.202104866
41. Wang T, Wang P, Pan L, et al. Stabling zinc metal anode with polydopamine regulation through dual effects of fast desolvation and ion confinement. *Adv Energy Mater*. 2023;13(5):2203523. https://doi.org/10.1002/aenm.202203523
42. Zheng J, Zhu G, Liu X, et al. Simultaneous dangling bond and zincophilic site engineering of SiN_x protective coatings toward stable zinc anodes. *ACS Energy Lett*. 2022;7(12):4443-4450. https://doi.org/10.1021/acsenergylett.2c02282
43. Yu H, Chen Y, Wei W, Ji X, Chen L. A functional organic zinc-chelate formation with nanoscaled granular structure enabling long-term and dendrite-free Zn anodes. *ACS Nano*. 2022;16(6):9736-9747. https://doi.org/10.1021/acsnano.2c03398
44. Liu H, Wang J-G, Hua W, et al. Navigating fast and uniform zinc deposition via a versatile metal-organic complex interphase. *Energy Environ Sci*. 2022;15(5):1872-1881. https://doi.org/10.1039/d2ee00209d

SUPPORTING INFORMATION

Additional supporting information can be found online in the Supporting Information section at the end of this article.

How to cite this article: Liu C, Zhu Y, Di S, et al. Crystallinity engineering of carbon nitride protective coating for ultra-stable Zn metal anodes. *Electron*. 2024;e29. https://doi.org/10.1002/elt2.29